



Title	Tumor Endothelial Cells Induce M2 Macrophage Polarization via IL-4, Enhancing Tumor Growth in Hepatocellular Carcinoma
Author(s)	Matoba, Daijiro; Noda, Takehiro; Kobayashi, Shogo et al.
Citation	Cancer Science. 2025
Version Type	VoR
URL	<a href="https://hdl.handle.net/11094/102952">https://hdl.handle.net/11094/102952</a>
rights	This article is licensed under a Creative Commons Attribution-NonCommercial-NoDerivatives 4.0 International License.
Note	








*The University of Osaka Institutional Knowledge Archive : OUKA*

<https://ir.library.osaka-u.ac.jp/>

The University of Osaka

## ORIGINAL ARTICLE OPEN ACCESS

# Tumor Endothelial Cells Induce M2 Macrophage Polarization via IL-4, Enhancing Tumor Growth in Hepatocellular Carcinoma

Daijiro Matoba<sup>1,2</sup> | Takehiro Noda<sup>1</sup>  | Shogo Kobayashi<sup>1</sup>  | Yoshihiro Sakano<sup>1</sup>  | Kenichi Matsumoto<sup>1</sup> | Chihiro Yamanaka<sup>1,3</sup> | Kazuki Sasaki<sup>1</sup> | Shinichiro Hasegawa<sup>1</sup> | Yoshifumi Iwagami<sup>1</sup> | Daisaku Yamada<sup>1</sup>  | Yoshito Tomimaru<sup>1</sup>  | Hirofumi Akita<sup>1</sup> | Hidenori Takahashi<sup>1</sup>  | Tadafumi Asaoka<sup>1,4</sup> | Junzo Shimizu<sup>1,5</sup> | Hisashi Wada<sup>2</sup> | Yuichiro Doki<sup>1</sup> | Hidetoshi Eguchi<sup>1</sup> 

<sup>1</sup>Department of Gastroenterological Surgery, Graduate School of Medicine, The University of Osaka, Osaka, Japan | <sup>2</sup>Department of Clinical Research in Tumor Immunology, Graduate School of Medicine, The University of Osaka, Osaka, Japan | <sup>3</sup>Department of Gastroenterological Surgery, Japan Community Health Care Organization Osaka Hospital, Osaka, Japan | <sup>4</sup>Department of Gastroenterological Surgery, Osaka International Medical & Science Center, Osaka Keisatsu Hospital, Osaka, Japan | <sup>5</sup>Department of Gastroenterological Surgery, Toyonaka Municipal Hospital, Osaka, Japan

**Correspondence:** Shogo Kobayashi ([s-kobayashi@umin.ac.jp](mailto:s-kobayashi@umin.ac.jp))

**Received:** 27 March 2025 | **Revised:** 23 July 2025 | **Accepted:** 12 August 2025

**Funding:** This work was supported in part by grants from Grant-in-Aid for Scientific Research of the Japan Society for the Promotion of Science (JSPS) [(C) 22K08870] and Grant-in-Aid for Young Scientists of the JSPS [(C) 22K16530]. The funders had no role in the study design, data collection and analysis, decision to publish, or preparation of the manuscript.

**Keywords:** immune suppression | tumor microenvironment | tumor vessel | tumor-associated macrophage | tumor-endothelial cells

## ABSTRACT

Tumor-associated macrophages (TAMs) and tumor endothelial cells (TECs) are important components in tumor microenvironments. This study examined the interaction between TECs and TAMs in hepatocellular carcinoma (HCC). The aim of this study is to clarify the mechanism of immune suppression and cancer progression mediated by the M2 polarization of TAMs. TECs were isolated from subcutaneous HCC tumors using murine BNL-T cells, and normal endothelial cells (NECs) were isolated from murine liver. M0 macrophages were obtained from bone marrow after incubation with M-CSF. Conditioned medium from TECs (TEC CM) or NECs (NEC CM) was added to M0 macrophages, and the polarization to M2 macrophages was assessed. The percentage of iNOS<sup>+</sup>CD206<sup>+</sup> cells was increased in the TEC CM group than in the NEC CM group. The subcutaneous tumor model with co-injection of BNL-T and TECs or NECs was applied, and the ratio of M2 macrophages (CD206<sup>+</sup>iNOS<sup>+</sup>CD45<sup>+</sup>CD11b<sup>+</sup>F4/80<sup>+</sup> cells) was elevated in the BNL-T + TEC group. IL-4 expression in TECs was upregulated compared to NECs, and the secretion of IL-4 was increased in the TEC CM compared to the NEC CM. After IL-4 down-regulation in TECs, the ratio of iNOS<sup>+</sup>CD206<sup>+</sup> cells decreased. The double immunofluorescent staining of CD31 and CD163 was performed in human HCC tissue. The number of CD31<sup>+</sup> endothelial cells correlated positively with CD163<sup>+</sup> TAMs. The high CD163/CD31 group showed poor prognosis in overall and disease-free survival. TECs induce M2 macrophage polarization through IL-4 secretion, leading to immune suppression and cancer progression.

**Abbreviations:** CM, conditioned medium; DFS, disease-free survival; EGM-2, Endothelial Cell Growth Medium 2-BulletKit; GPNMB, glycoprotein non-metastatic gene B; HCC, hepatocellular carcinoma; HPF, high power field; IFN, interferon; M-CSF, macrophage colony-stimulating factor; NEC, normal endothelial cell; OS, overall survival; RT-qPCR, reverse-transcription quantitative polymerase chain reaction; STAT, signal transducer and activator of transcription; TAM, tumor-associated macrophage; TEC, tumor endothelial cell; TGF, transforming growth factor; TME, tumor microenvironment.

This is an open access article under the terms of the [Creative Commons Attribution-NonCommercial-NoDerivs](https://creativecommons.org/licenses/by-nc-nd/4.0/) License, which permits use and distribution in any medium, provided the original work is properly cited, the use is non-commercial and no modifications or adaptations are made.

© 2025 The Author(s). *Cancer Science* published by John Wiley & Sons Australia, Ltd on behalf of Japanese Cancer Association.

## 1 | Introduction

Hepatocellular carcinoma (HCC) is a major cause of cancer-related death worldwide [1]. Despite therapeutic advances, HCC prognosis remains poor due to high recurrence [2, 3]. Recently, combination therapy with immune checkpoint inhibitors and anti-angiogenic therapy, such as atezolizumab and bevacizumab, has emerged as a promising treatment option for advanced HCC [4]. Atezolizumab blocks PD-L1, enhancing T-cell response. Bevacizumab targets VEGF, inhibiting angiogenesis and promoting tumor vessel normalization [5]. The combination therapy of atezolizumab and bevacizumab with these two distinct mechanisms has demonstrated a synergistic therapeutic effect in tumor microenvironments (TMEs) containing cancer cells, endothelial cells, and immune cells [6–8].

Both tumor-associated macrophages (TAMs) and tumor endothelial cells (TECs) are important components of TMEs. Macrophages include TAMs derived from mononuclear cells, tissue-resident macrophages, and myeloid-derived suppressor cells. TAMs, the most abundant immune cells in tumors, polarize into M1 or M2 subtypes. The M2 macrophages promote tumor progression in several solid cancers such as HCC, by enhancing angiogenesis and immune evasion in the TME via anti-inflammatory cytokines [9–12]. These findings suggest TAMs interactions with stromal cells contribute to M2-driven tumor progression.

TECs adhere less to pericytes than normal endothelial cells (NECs) [13], disrupting vasculature and aiding metastasis [14, 15]. RK Jain proposed the concept of ‘tumor vessel normalization’, stabilizing abnormal vasculature as a promising treatment strategy [16]. Previously, we reported TECs glycolysis inhibition induces tumor vessel normalization in HCC model and tumor vasculature was related to poor prognosis in HCC [17]. Moreover, we demonstrated that the interaction between TECs and infiltrating T cells via glycoprotein non-metastatic gene B (GPNMB) induces T-cell exhaustion [18]. However, the cellular interaction between TECs and TAMs remains unclear.

We hypothesize that TECs promote the polarization of TAMs into the M2 subtype, contributing to a more immunosuppressive and tumor-promoting environment. To test this hypothesis, we conducted a series of in vitro and in vivo experiments to comprehensively assess the impact of TECs on the behavior of TAMs. This study aimed to investigate the cellular interaction between TECs and TAMs and to clarify the mechanism of immune suppression mediated by the polarization of TAMs toward the M2 phenotype in HCC.

## 2 | Materials and Methods

### 2.1 | Cancer Cell Lines and Establishing a Highly Tumorigenic Cell Line

We used the murine HCC cell line BNL 1ME A.7R.1 (BNL), which was obtained from the ATCC (Virginia, USA). Cells were cultured in DMEM with 10% FBS. To establish a highly

tumorigenic cell line (BNL-T),  $5 \times 10^5$  BNL cells were injected subcutaneously into Balb/cAJcl-nu/nu mice (CLEA Japan, Tokyo, Japan). We used nude mice for the establishment of BNL-T because BNL cells have a low engraftment rate in immunocompetent mice, and nude mice allowed for more reliable tumor formation [17]. After 2 weeks, the tumors were minced, and the collected cells were cultured in DMEM. These cells were then reinjected subcutaneously into mice. After 3 cycles, cells were named BNL-T.

### 2.2 | Endothelial Cell Isolation and Functional Analysis

To isolate TECs and NECs,  $5 \times 10^5$  BNL-T cells were injected subcutaneously into 8-week-old BALB/cAJcl-nu/nu mice. We used nude mice since tumor growth was more robust, resulting in improved efficiency in isolating TECs [17]. After 2 weeks, tumors and normal liver tissue were harvested. Tissues were digested for single-cell suspension. The cells were subsequently labeled with anti-CD31 antibody-coated magnetic beads (Miltenyi Biotec, Bergisch Gladbach, Germany) for 15 min. After washing, CD31<sup>+</sup> cells were collected using a QuadroMACS system (Miltenyi Biotec). These cells were cultured in EGM-2 (Lonza, Verviers, Belgium), the medium for vascular endothelial cells. To assess their tube-forming ability, the TECs or NECs were incubated for 24 h in a 6-well dish coated with Matrigel Matrix (Corning, NY, USA).

### 2.3 | Immunocytochemical Staining

Immunocytochemistry was performed as described previously [19]. Briefly, cells stained with anti-CD31 (Abcam, Cambridge, UK) and DAPI were imaged by fluorescence microscope (BX-X700; Keyence, Osaka, Japan).

### 2.4 | Western Blotting

Western blotting followed previous methods [20]. We used anti-CD31 (Abcam) and anti- $\beta$ -actin antibodies (Sigma-Aldrich). For detection, we used horseradish peroxidase-conjugated anti-rabbit IgG (GE Healthcare Biosciences, Marlborough, MA, USA) and the ECL Prime Western Blotting Detection kit (GE Healthcare Biosciences).

### 2.5 | Isolation of M0 Macrophages From Bone Marrow

Femurs and tibias were harvested from BALB/cAJcl mice, and bone marrow was collected. The single-cell suspension was seeded onto Repcell plates (CellSeed Inc., Tokyo, Japan). RPMI 1640 medium supplemented with 10% FBS, 10 ng/mL recombinant mouse M-CSF (R&D), 1% MEM Non-Essential Amino Acid Solution, and 1% GlutaMAX Supplement (Gibco) was used as the growth medium for bone marrow-derived macrophages. M0 macrophages were harvested on day 7, with medium changed on day 3.

## 2.6 | Reverse Transcription Quantitative-Polymerase Chain Reaction (RT-qPCR)

RT-qPCR was performed as described previously [21]. Briefly, RNA extraction and reverse transcription used the Promega Reverse Transcriptase System Kit (Promega, Madison, WI, USA). RT-qPCR was then performed using the ViiA7 Real-Time PCR system (Thermo Fisher Scientific, Waltham, MA, USA). Amplification was achieved with the THUNDERBIRD SYBR qPCR Mix (Toyobo, Osaka, Japan). We selected IL-10, Arginase-1, and TGF- $\beta$ 1 as genes that are characteristically expressed in M2 macrophages [9]. Additionally, previous reports have identified IL-4, IL-10, IL-13, and TGF- $\beta$ 1 as representative cytokines that directly polarize macrophages into the M2 phenotype. We analyzed the gene expression of TEC and NEC in relation to these cytokines [22, 23]. Gene expression levels were normalized to *Gapdh*. The following primers were used: *Gapdh*, 5'—TGCCCCATGTTTGTGATG—3' (forward) and 5'—TGTGGTCATGAGCCCTTCC—3' (reverse); *Il-10*, 5'—CTTACTGACTGGCATGAGGATCA—3' (forward) and 5'—GCAGCTCTAGGAGCATGTGG—3' (reverse); *Arginase-1*, 5'—CTCCAAGCCAAAGTCCTTAGAG—3' (forward) and 5'—GGAGCTGTCATTAGGGACATCA—3' (reverse); *Tgf- $\beta$ 1*, 5'—CCACCTGCAAGACCATCGAC—3' (forward) and 5'—CTGGCGAGCCTTAGTTTGGAC—3' (reverse); *Il-4*, 5'—GGTCTCAACCCCAAGCTAGT—3' (forward) and 5'—GCCGATGATCTCTCTCAAGTGAT—3' (reverse); *Il-13*, 5'—TGAGCAACATCACACAAGACC—3' (forward) and 5'—GGCCTTGCGGTTACAGAGG—3' (reverse).

## 2.7 | Flow Cytometry

Cells were stained with fluorescence-conjugated antibodies following staining using viability dye (Thermo Fisher Scientific). For intracellular staining, the BD Pharmingen Transcription Factor Buffer Set (BD Biosciences, Franklin Lakes, NJ, USA) was utilized. The gating strategy of flow cytometry is shown in Figure S1A (in vitro experiments) and S1B (in vivo experiments). Briefly, in vitro, the purified samples were sequentially gated on live cells, single cells, CD11b, and F4/80. We defined CD11b<sup>+</sup>F4/80<sup>+</sup> cells as macrophages. In vivo, the purified samples were sequentially gated on live cells, single cells, CD45, CD11b, and F4/80. We defined CD45<sup>+</sup>CD11b<sup>+</sup>F4/80<sup>+</sup> cells as macrophages. The antibodies included anti-CD45, anti-F4/80, anti-CD11b, anti-CD206, and anti-inducible nitric oxide synthase (iNOS), all purchased from BioLegend. Flow cytometry was performed using Novocyte (Agilent, Santa Clara, CA, USA) and analyzed by Novo Express software (Agilent).

## 2.8 | Evaluation of Macrophage Polarization In Vitro

M0 macrophages were developed from murine bone marrow. Conditioned medium (CM) was collected from the supernatant of the TECs (TEC CM) or NECs (NEC CM). The M0 macrophages were cultured in a 1:1 ratio with TEC CM or NEC CM in the bone marrow-derived macrophage growth medium. Macrophage polarization was assessed using RT-qPCR and flow cytometry.

Macrophages were identified as F4/80<sup>+</sup>CD11b<sup>+</sup> cells, and M2 macrophages were defined as CD206<sup>+</sup>iNOS<sup>+</sup>F4/80<sup>+</sup>CD11b<sup>+</sup> cells. Cells cultured with bone marrow-derived macrophage growth medium containing 10 ng/mL recombinant mouse IL-10 (R&D) were used as a positive control.

## 2.9 | Animal Experiments

Animal experiments were performed using 8-week-old male BALB/cAJcl mice (CLEA Japan). For in vivo tumor formation, BALB/cAJcl mice were injected subcutaneously with  $5 \times 10^5$  BNL-T cells (BNL-T group),  $4.5 \times 10^5$  BNL-T cells +  $5 \times 10^4$  NECs (BNL-T + NECs group), or  $4.5 \times 10^5$  BNL-T cells +  $5 \times 10^4$  TECs (BNL-T + TECs group) ( $N = 5$  per group). After 2 weeks, the tumors were harvested and tumor weight assessed. Tumors were subjected to fluorescent double immunostaining to evaluate the endothelial cells and macrophages. CD206 was used as a marker for M2 macrophages, CD31 for endothelial cells, and CD80 for M1 macrophages. Ten high-magnification fields were randomly selected, and macrophage counts were compared across groups.

For RT-qPCR and flow cytometry, tumors were dissociated into single cells. To assess gene expression of *Il-10*, *Arginase-1*, and *Tgf- $\beta$ 1* in macrophages, CD45<sup>+</sup>F4/80<sup>+</sup>CD11b<sup>+</sup> cells were collected using a FACS Aria II (BD Bioscience).

For flow cytometry, cells were stained with anti-CD45, anti-F4/80, anti-CD11b, anti-CD206, and anti-iNOS antibodies. M2 macrophages were assessed as iNOS<sup>+</sup>CD206<sup>+</sup>CD45<sup>+</sup>F4/80<sup>+</sup>CD11b<sup>+</sup> cells, and the ratio of M2 macrophages among all intratumoral macrophages (CD45<sup>+</sup>F4/80<sup>+</sup>CD11b<sup>+</sup> cells) was evaluated.

## 2.10 | Immunofluorescent Staining

The immunostaining methods were performed as previously described [17, 24]. The following primary antibodies were used: anti-F4/80 (Abcam), anti-CD80 (Invitrogen), anti-CD31, anti-CD206 (Abcam), anti-CD163 (Novus Biologicals, Littleton, CO, USA), and anti-IL-4 (Cusabio, Wuhan Huamei Biotech Co. Ltd., Wuhan, China). Tissue sections were stained with Alexa Fluor-488- or Alexa Fluor-647-conjugated secondary immunoglobulin G (Cell Signaling Technology, Danvers, MA, USA). Nuclei were counterstained with DAPI. Images were captured using a BZ-X700 microscope and analyzed by BZ-X Analyzer software (Keyence).

## 2.11 | Elisa

IL-4, IL-10, and TGF- $\beta$ 1 levels in the supernatant of culture medium from TECs, NECs, M0 macrophages, and M0 macrophages cultured with NEC CM or TEC CM were measured using a mouse IL-4, IL-10, and TGF- $\beta$ 1 ELISA kit (R&D). Briefly, culture supernatants were collected from TECs or NECs, M0 macrophages, and M0 macrophages cultured with NEC CM or TEC CM, and the protein levels were measured following the instructions provided in the ELISA kits.



## 2.12 | Downregulation of *IL-4* Gene Expression by Small Interfering RNA

To downregulate *IL-4* expression, TECs were transfected with 5 nM siRNA (Silencer Select Pre-Designed siRNA, Invitrogen) using

Lipofectamine RNAiMAX reagent (Invitrogen). As a control, non-targeting siRNA (scramble siRNA, Silencer Select negative control #1 siRNA; Life Technologies) was transfected. *IL-4* downregulation was confirmed by RT-qPCR and by measuring the IL-4 concentration in the culture supernatant using ELISA. To assess

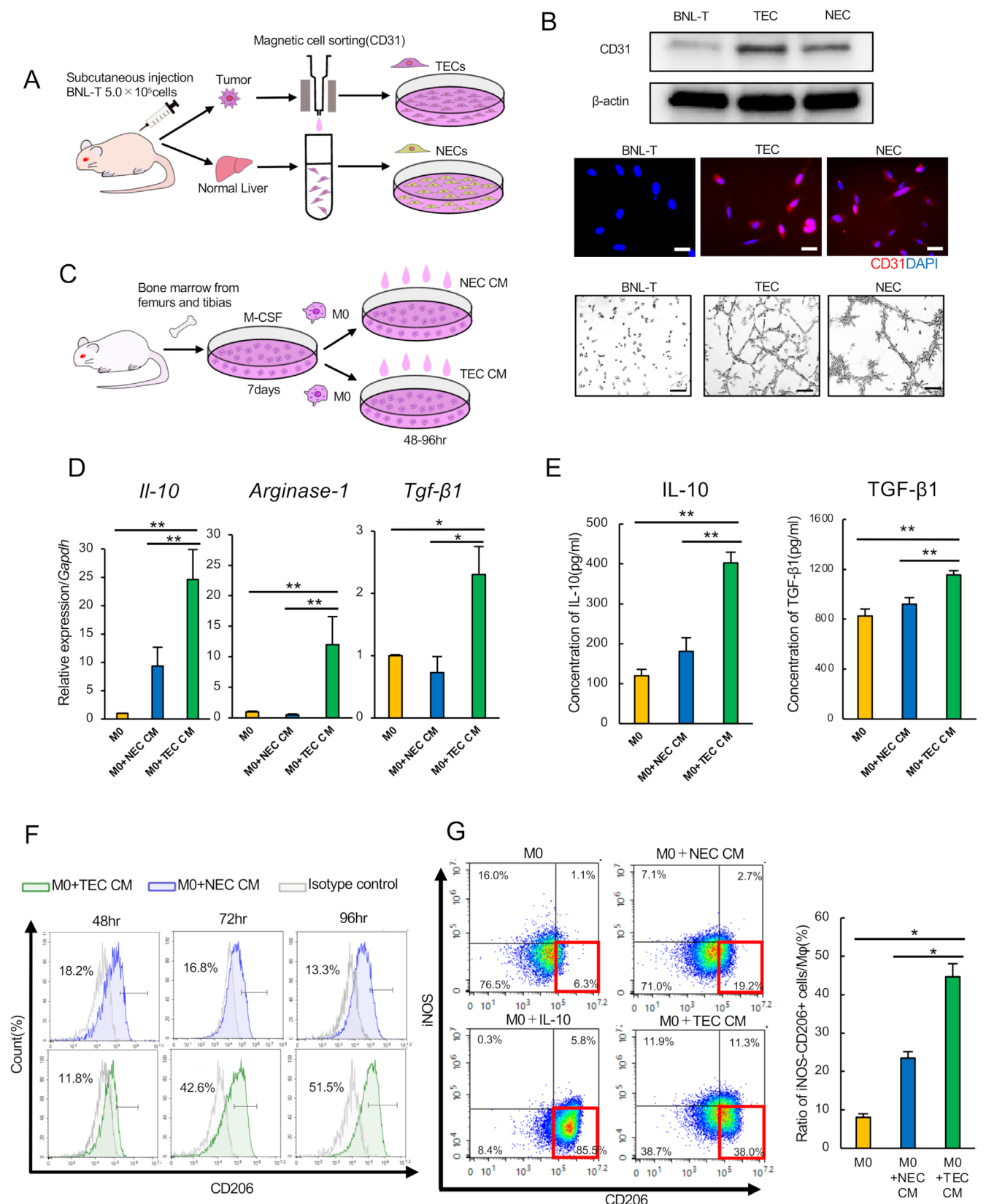


**FIGURE 1** | Legend on next page.

**FIGURE 1** | Isolation of cells and evaluation of macrophage polarity. (A) TEC and NEC isolation from BNL-T tumors or normal livers using magnetic cell sorting. (B) Western blot analysis of CD31 (top). Immunocytochemical analysis of CD31. Nuclei were counterstained with DAPI (scale bars, 50  $\mu$ m) (middle). Tube formation assay (scale bars, 100  $\mu$ m) (bottom). (C) Isolation of bone marrow-derived macrophages and evaluation of macrophage polarity. (D) RT-qPCR after culture with conditioned medium (CM) from NEC or TEC. (E) ELISA of IL-10 and TGF- $\beta$ 1 in the supernatants of M0, M0 + NEC CM, and M0 + TEC CM ( $N=3$ ). (F) Flow cytometric analysis of CD206 after incubation with CM from TEC or NEC. (G) Flow cytometric analysis of CD206 and iNOS expression by M0, M0 cultured with CM from TEC or NEC, and IL-10 as positive control (left panel). The percentage of CD206<sup>+</sup>iNOS<sup>-</sup> cells among total macrophages is shown in the right panel ( $N=4$ ). Mean  $\pm$  SEM. \* $p < 0.05$ ; \*\* $p < 0.01$ .

*Il-4* downregulation effects, M0 macrophages were cultured with supernatants from si*Il-4* TECs, siScramble TECs, or si*Il-4* TECs with recombinant IL-4 (1 ng/mL) and analyzed by flow cytometry. For the in vivo experiments, BALB/cA/Jcl mice were injected subcutaneously with either BNL-T cells + TECs with scramble siRNA or BNL-T cells + TECs with *Il-4* siRNA. Tumor weights were compared, and M2 macrophage counts were assessed by fluorescent double immunostaining for CD31 and CD206 as described above.

### 2.13 | Clinical Tissue Samples

Formalin-fixed paraffin-embedded HCC samples were obtained from 73 patients who underwent hepatectomy at the University of Osaka Hospital, between 2010 and 2013. Fluorescent double immunostaining was performed on the HCC samples to quantify CD163<sup>+</sup> and CD31<sup>+</sup> cells. The median value for each marker was used to divide the patients into four groups to analyze the clinicopathological factors and prognosis. Furthermore, 42 cases were selected from this cohort, and double fluorescent immunostaining for CD31, CD206, and IL-4 was performed. The numbers of CD31 and CD206 were counted, and their correlation with prognosis was evaluated. In addition, the localization of IL-4-positive cells was evaluated.

### 2.14 | Statistical Analysis

The clinicopathological variables of the patients were analyzed using chi-squared tests for categorical data, whereas continuous variables were compared using Student's *t*-tests. Nonparametric tests, specifically the Mann-Whitney *U* test, were carried out to assess the significance of differences between groups. Kaplan-Meier curves were used to analyze disease-free survival (DFS) and overall survival (OS), with differences assessed by the log-rank test. Univariate and multivariate analyses of prognostic factors utilized a Cox proportional hazards model. Statistical analyses were performed using JMP software version 17.2 (SAS Institute Inc., Cary, NC, USA).

## 3 | Results

### 3.1 | Isolation of Tumor and Normal Endothelial Cells From Murine Subcutaneous Tumor Model

The procedure is shown in Figure 1A. Western blotting confirmed CD31 expression in TECs and NECs (Figure 1B, top panel). Immunocytochemistry showed strong CD31 expression in TECs and NECs compared to BNL-T cells (Figure 1B, middle

panel). In the tube formation assay, TECs and NECs formed round tubes typical of cultured endothelial cells, whereas BNL-T cells did not exhibit tube formation (Figure 1B, bottom panel). These findings confirm the successful isolation of NECs and TECs.

### 3.2 | Isolation of Bone Marrow-Derived Macrophages and Evaluation of Macrophage Polarity

We collected bone marrow from the femurs and tibias of mice and harvested M0 macrophages after differentiation with M-CSF for 7 days. TEC CM and NEC CM were added to M0 macrophages, and the cells were collected after incubation. The procedure is illustrated in Figure 1C. The expression of *Il-10*, *Arginase-1*, and *Tgf- $\beta$ 1* was significantly upregulated in the group treated with TEC CM (M0 + TEC CM) compared with both M0 macrophages and the group treated with NEC CM (M0 + NEC CM) (Figure 1D). In addition, the concentrations of IL-10 and TGF- $\beta$ 1 in the supernatant were also significantly higher in M0 + TEC CM than in M0 and M0 + NEC CM (Figure 1E). In flow cytometric analysis, the percentage of CD206<sup>+</sup> macrophages reached 42.6% and 51.5% in the M0 + TEC CM group but did not change in the M0 + NEC CM group (16.8% and 13.3%, respectively) (Figure 1F). iNOS is one of the markers of M1 macrophages, and the percentages of iNOS<sup>+</sup>CD206<sup>+</sup> cells among macrophages were higher in cells treated with TEC CM (38.0%) than those treated with NEC CM (19.2%). These results indicate that M0 macrophages were polarized to the M2 phenotype more by TEC CM than NEC CM (Figure 1G).

### 3.3 | Evaluation of the Effect of Tumor Endothelial Cells on Tumor Growth and Intratumoral Macrophage Polarity In Vivo

The subcutaneous tumor models were analyzed to evaluate the effect of TECs on tumor growth and intratumoral macrophage polarity. An overview of the experiments is presented in Figure 2A. BNL-T + TECs tumors were significantly heavier than BNL-T alone or the BNL-T + NECs group. Figure 2B shows tumor appearance (left) and the average weights in the three groups ( $p < 0.01$ , right). Double immunofluorescent staining of CD206 and CD31 showed that the number of CD206<sup>+</sup> M2 macrophages was significantly higher in the BNL-T + TECs group (18.1 cells/HPF) compared with the BNL-T (9.8 cells/HPF) and BNL-T + NECs (12.0 cells/HPF) groups ( $p < 0.01$ , Figure 2C). Conversely, the number of CD80<sup>+</sup> M1 macrophages was reduced in the BNL-T + TECs group (2.9 cells/HPF) compared with the BNL-T (9.8 cells/HPF) and

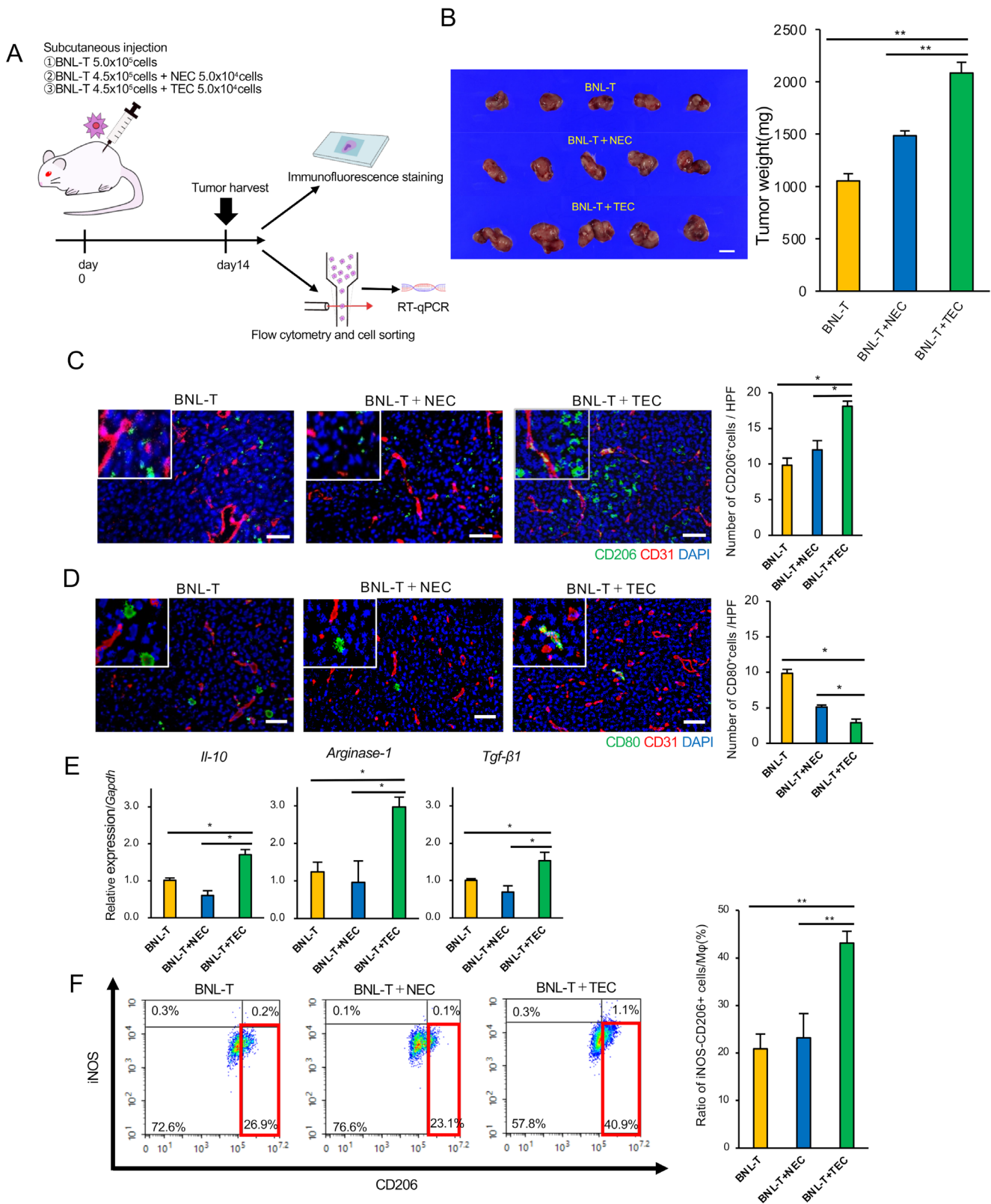


**FIGURE 2** | The effect of TECs on tumor growth and intratumoral macrophage polarity. (A) An overview of the experimental subcutaneous tumor model established by BNL-T alone, a mixture of BNL-T + NEC, and a mixture of BNL-T + TEC. (B) Tumor images and weight comparison ( $N = 5$ ) (scale bars, 10 mm). (C) Double immunofluorescent staining of CD31 and CD206. Nuclei were counterstained with DAPI. Quantification of CD206<sup>+</sup> cells (right) (scale bars, 100  $\mu$ m). (D) Double immunofluorescent staining of CD31 and CD80. Quantification of CD80<sup>+</sup> cells (right) (scale bars, 100  $\mu$ m). (E) RT-qPCR in intratumoral macrophages. (F) Flow cytometry of CD206/iNOS in macrophages from BNL-T, BNL-T + NEC, and BNL-T + TEC tumors (left panel). The percentage of CD206<sup>+</sup>iNOS<sup>+</sup> cells among the total intratumoral macrophages is shown in the right panel ( $N = 5$ ). Mean  $\pm$  SEM. \* $p < 0.05$ ; \*\* $p < 0.01$ .

BNL-T+NECs (5.1 cells/HPF) groups ( $p < 0.01$ , Figure 2D). However, in the F4/80 and CD31 fluorescent double-staining, there was no significant difference in the total number of macrophages among the three groups (Figure S2A). The expression of *Il-10*, *Arginase-1*, and *Tgf- $\beta$ 1* was upregulated in BNL-T+TECs (Figure 2E). Flow cytometric analysis of the tumors revealed a significantly higher percentage of M2 macrophages (CD206<sup>+</sup>iNOS<sup>-</sup>CD45<sup>+</sup>CD11b<sup>+</sup>F4/80<sup>+</sup> cells) among all macrophages in the BNL-T+TECs group (40.9%) compared with the BNL-T (26.9%) and BNL-T+NECs (23.1%) groups ( $p < 0.01$ , Figure 2F). These results indicate that a specific factor from TECs influenced M2 macrophage polarization.

### 3.4 | Examination of a Specific Factor From Tumor Endothelial Cells Promoting M2 Macrophage Polarization

To examine a specific factor from TECs that promotes M2 macrophage polarization, RT-qPCR for *Il-4*, *Il-10*, *Il-13*, and *Tgf- $\beta$ 1* was performed for BNL-T cells, NECs, and TECs. ELISA of IL-4 and IL-10 was also performed with BNL-T, NEC, and TEC supernatant (Figure 3A). The analysis of mRNA expression revealed that *Il-4* was significantly upregulated in TECs compared to NECs and BNL-T cells ( $p < 0.01$ ). *Il-13* was also upregulated in TECs compared to BNL-T cells, though the difference from NECs was not significant. The expression levels of *Il-10* and *Tgf- $\beta$ 1* were not significant in the three groups

(Figure 3B). ELISA showed TECs secreted a significantly higher level of IL-4 (2000 pg/mL) than BNL-T (165 pg/mL) and NECs (270 pg/mL) ( $p < 0.01$ ). The secretion of IL-10 was minimal across all cell types, with no significant differences observed (Figure 3C).

### 3.5 | IL-4 Down-Regulation in Tumor Endothelial Cells Suppressed M2 Macrophage Polarization, Which Was Restored by Recombinant IL-4

We prepared the CM from TECs after down-regulation of *Il-4* expression, and M0 macrophages were incubated with CM from TECs treated with scramble siRNA or *Il-4* siRNA. M2 polarization was assessed by flow cytometry (Figure 4A). After treatment of TECs with *Il-4* siRNA, *Il-4* expression was significantly suppressed ( $p < 0.01$ ), and ELISA confirmed IL-4 reduction ( $p < 0.01$ ) (Figure 4B). Flow cytometric analysis revealed that CM from TECs treated with *Il-4* siRNA had a decreased ratio of iNOS<sup>-</sup>CD206<sup>+</sup> cells (10.4%) compared to treatment with scramble siRNA (39.6%). Moreover, adding recombinant IL-4 restored iNOS<sup>-</sup>CD206<sup>+</sup> cells to 40.5% (Figure 4C). We also established a mouse subcutaneous tumor model using BNL-T+TECs with *Il-4* siRNA (Figure 4D). The macroscopic appearance of the tumors is shown in Figure 4E (left panel), and the average tumor weights in the BNL-T+TECs with scramble siRNA model and BNL-T+TECs with *Il-4* siRNA model were 1,918 mg and 1,477 mg, respectively ( $p < 0.01$ ; Figure 4E, right panel). Double

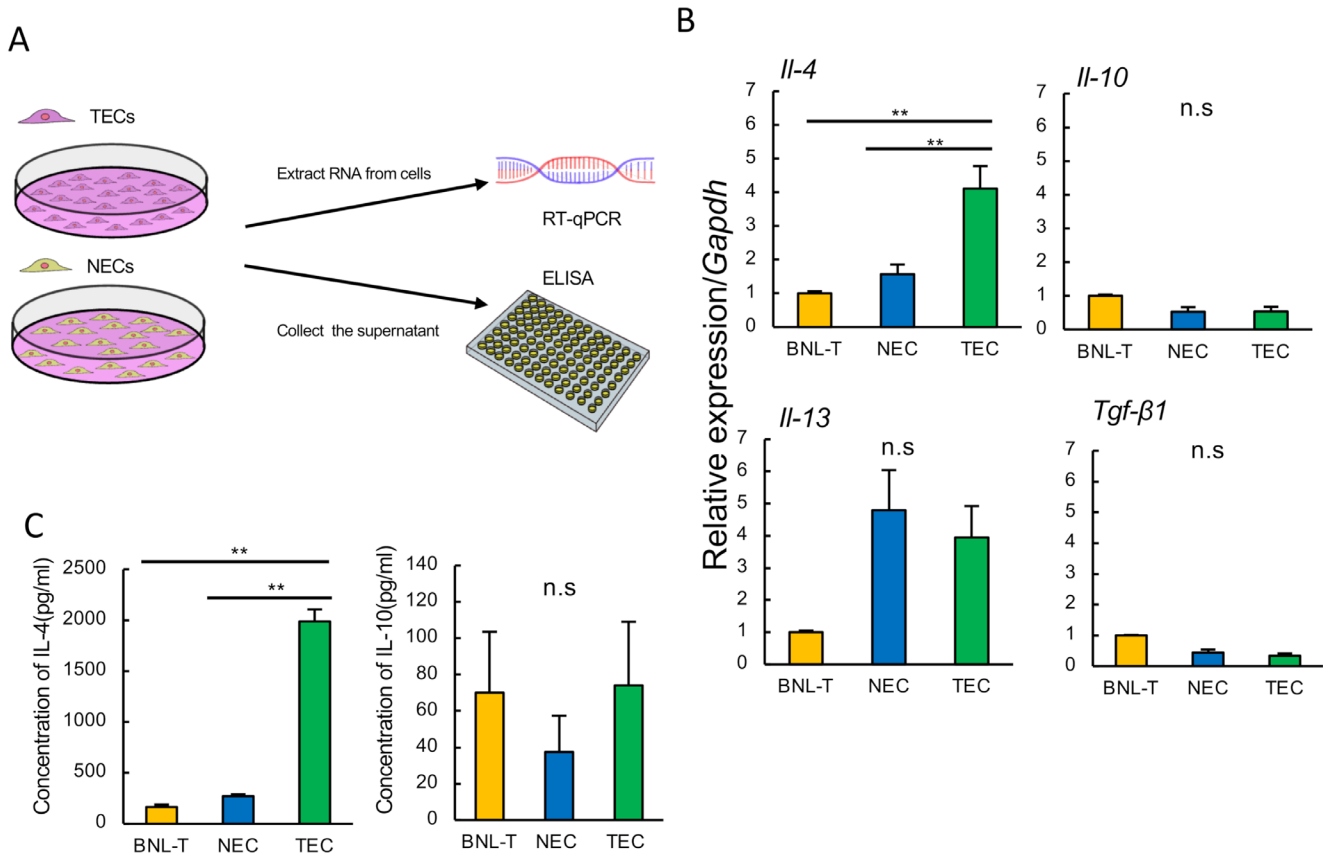


**FIGURE 3** | Examination of a specific factor from TECs promoting M2 macrophage polarization. (A) Experimental schema for RT-qPCR and ELISA. (B) RT-qPCR of BNL-T, NECs, and TECs. (N=3) (C) ELISA of IL-4 and IL-10 in the supernatants of BNL-T, NECs, and TECs. (N=3) Mean  $\pm$  SEM. \* $p < 0.05$ ; \*\* $p < 0.01$ , n.s;  $p > 0.05$ .



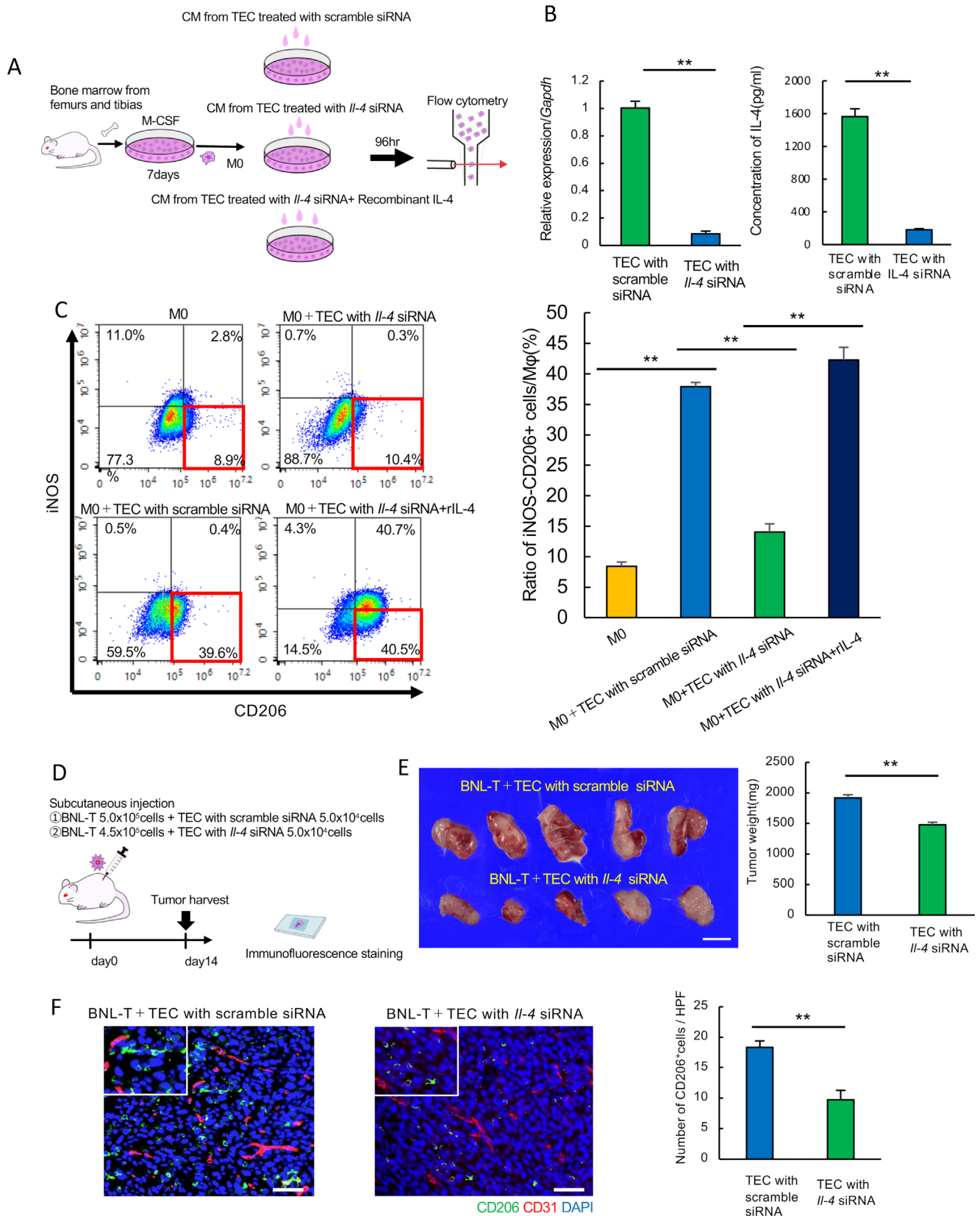


**FIGURE 4** | Legend on next page.

immunofluorescent staining of CD206 and CD31 showed that the number of CD206<sup>+</sup> cells was significantly lower in the BNL-T + TECs treated with *IL-4* siRNA model (9.7 cells/HPF) than in the BNL-T + TECs treated with scramble siRNA model

(18.3 cells/HPF) ( $p < 0.01$ ; Figure 4F). But in the F4/80 and CD31 fluorescent double-staining, there was no significant difference in the total number of macrophages among the two groups (Figure S2B).



**FIGURE 4** | *IL-4* downregulation in TECs and the effect on M2 macrophage polarity. (A) Schema of the flow cytometric analysis of isolated macrophages cultured with conditioned medium (CM) from TEC treated with scramble siRNA or *IL-4* siRNA. (B) RT-qPCR of *IL-4* in TECs (left). ELISA of *IL-4* in CM from TEC (right). (C) Flow cytometric analysis of CD206 and iNOS expression of M0, M0 cultured with CM from TECs treated with scramble siRNA, *IL-4* siRNA, and the addition of recombinant *IL-4* (left panel) ( $N=4$ ). The percentage of CD206<sup>+</sup>iNOS<sup>-</sup> cells in total macrophages is shown in the right panel. (D) Experimental scheme for the subcutaneous tumor model established using BNL-T + TEC with scramble siRNA and BNL-T + TEC with *IL-4* siRNA. (E) Macroscopic appearance of the tumors (scale bars, 10 mm) and comparison of tumor weights. ( $N=5$ ) (F) Double immunofluorescent staining of CD31 and CD206. Nuclei were counterstained with DAPI (scale bars, 100  $\mu$ m). Quantification of CD206-positive cells in the tumor (right) Mean  $\pm$  SEM. \*\* $p < 0.01$ .

### 3.6 | Analysis of the Relationship Between the Number of M2 Macrophages and Tumor Blood Vessels in HCC Tissues

CD31<sup>+</sup> cells were identified as vascular endothelial cells, and CD163<sup>+</sup> cells represented M2 macrophages. Patients were divided into two groups based on the median number of CD31<sup>+</sup> cells (median value, 13 cells/HPF). Representative figures for each case with a low and high number of CD31<sup>+</sup> cells are shown in Figure 5A. In the group of high (> 13) CD31<sup>+</sup> cells, the number of CD163<sup>+</sup> cells was significantly higher (17.6 vs. 7.6 cells/HPF,  $p < 0.05$ ). A scatter plot demonstrated a positive correlation between the number of CD31<sup>+</sup> cells and CD163<sup>+</sup> cells ( $r=0.61$ ) (Figure 5B). Using the median values for both CD31<sup>+</sup> cells and CD163<sup>+</sup> cells, patients were further categorized into four groups: a group with high CD31<sup>+</sup> cells and high CD163<sup>+</sup> cells (high CD163 and high CD31), two groups with a high number of one of the cells (high CD163 and low CD31; low CD163 and high CD31), and a group with low numbers of both (low CD163 and low CD31). Representative double immunofluorescent staining is shown in Figure 5C. In fluorescent double immunostaining with CD31 and IL-4, IL-4 was specifically expressed in CD31-positive cells and was not expressed in low CD31 cases (Figure 5D). We compared clinicopathological factors and prognosis between two groups: high CD163 and high CD31 versus the other. A comparison of patient characteristics between the two groups is presented in Table 1. The group with high CD163 and high CD31 had elevated serum alpha-fetoprotein levels ( $p=0.001$ ) and a higher incidence of microscopic vascular invasion ( $p=0.040$ ) compared to the other group. There were no significant differences in other factors. Kaplan–Meier analysis revealed that the high CD163 and high CD31 group had significantly lower OS and DFS rates compared with the other group (5-year OS: 30.8% vs. 80.9%, 5-year DFS: 15.7% vs. 49.7%,  $p < 0.0001$ ; Figure 5E). Figure S3 showed the prognostic analysis of DFS and OS among the four groups (2-year DFS: 20.8% in high CD163 and high CD31, 33.3% in high CD163 and low CD31, 57.1% in low CD163 and high CD31, and 80.7% in low CD163 and low CD31,  $p < 0.0001$ ; 5-year OS: 30.8% in high CD163 and high CD31, 66.7% in high CD163 and low CD31, 83.3% in low CD163 and high CD31, and 84.4% in low CD163 and low CD31,  $p < 0.0001$ ). Furthermore, univariate and multivariate analyses demonstrated that CD163 and CD31 expression were independently significant prognostic factors for both OS (hazard ratio, 4.880;  $p < 0.001$ , Table 2) and DFS (hazard ratio, 3.358;  $p < 0.001$ , Table 3). In addition, double immunofluorescent staining was conducted using CD31 and CD206 (Figure S4A), and the results showed that the high CD206 and high CD31 groups had the worst OS and DFS (5-year OS: 37.8% vs. 69.8%,  $p < 0.05$ , 5-year DFS: 20.8% vs. 38.7%,

$p < 0.05$ ; Figure S4B), which was consistent with the results of the CD163 study.

## 4 | Discussion

This study demonstrated that TECs induce M2 polarization via IL-4, promoting immune suppression in HCC. Clinical analysis showed TECs correlated with M2 macrophages, and the combination of high levels of both was identified as a poor prognostic factor in HCC patients.

In HCC tissues, multidimensional analysis revealed that a special TME exists and various types of cells in the TME contribute to tumor progression, including TAMs, CD4<sup>+</sup> T cells, cytotoxic T lymphocytes, regulatory T cells, dendritic cells, and tumor-endothelial cells. Among these, TAMs enhance tumor growth by suppressing immunity and promoting angiogenesis. High TAM density predicts poor prognosis post-resection in HCC [25, 26]. TAMs can be divided into M1 and M2 subtypes, and M1 macrophages are mainly induced by lipopolysaccharide and interferon (IFN)- $\gamma$ , and the M1 subtype inhibits tumor progression. M2 macrophages exert immunomodulatory functions, which possess cancer-promoting and anti-inflammatory effects by triggering immunosuppression. Therefore, they have emerged as therapeutic targets in cancer therapy, and therapeutic interventions targeting the M2 polarization of TAMs are currently under investigation [27–29]. It was supposed that M2 macrophages are induced by T-helper 2 (Th2) cytokines IL-4, IL-10, and IL-13, but the actual mechanism of macrophage polarization is still unclear because the crosstalk between macrophage polarization and the microenvironment is very intense and complicated. Although not analyzed in this study, it has been reported that M2 polarization of TAMs is also related to tumor vascular normalization. Rolny et al. reported that the host-produced histidine-rich glycoprotein promoted antitumor immune responses and vessel normalization by inhibiting M2 macrophage polarization. Peng et al. also demonstrated that the polarization of TAMs is associated with tumor vascular normalization induced by endostatin in lung cancer [30, 31]. In this study, we showed that TECs induce M2 macrophage polarization through IL-4 secretion in HCC, and the high number of both TECs and M2 macrophages in the HCC tissue correlates with poor prognosis. Our data suggest that targeting IL-4 secreted from TECs could be a promising treatment strategy for HCC.

IL-4 is a multifunctional cytokine primarily secreted by activated Th2 cells and plays a pivotal role in regulating immune responses, including Th2 cell differentiation, mucus secretion, and eosinophil activation. In the context of cancer, IL-4, IL-10,

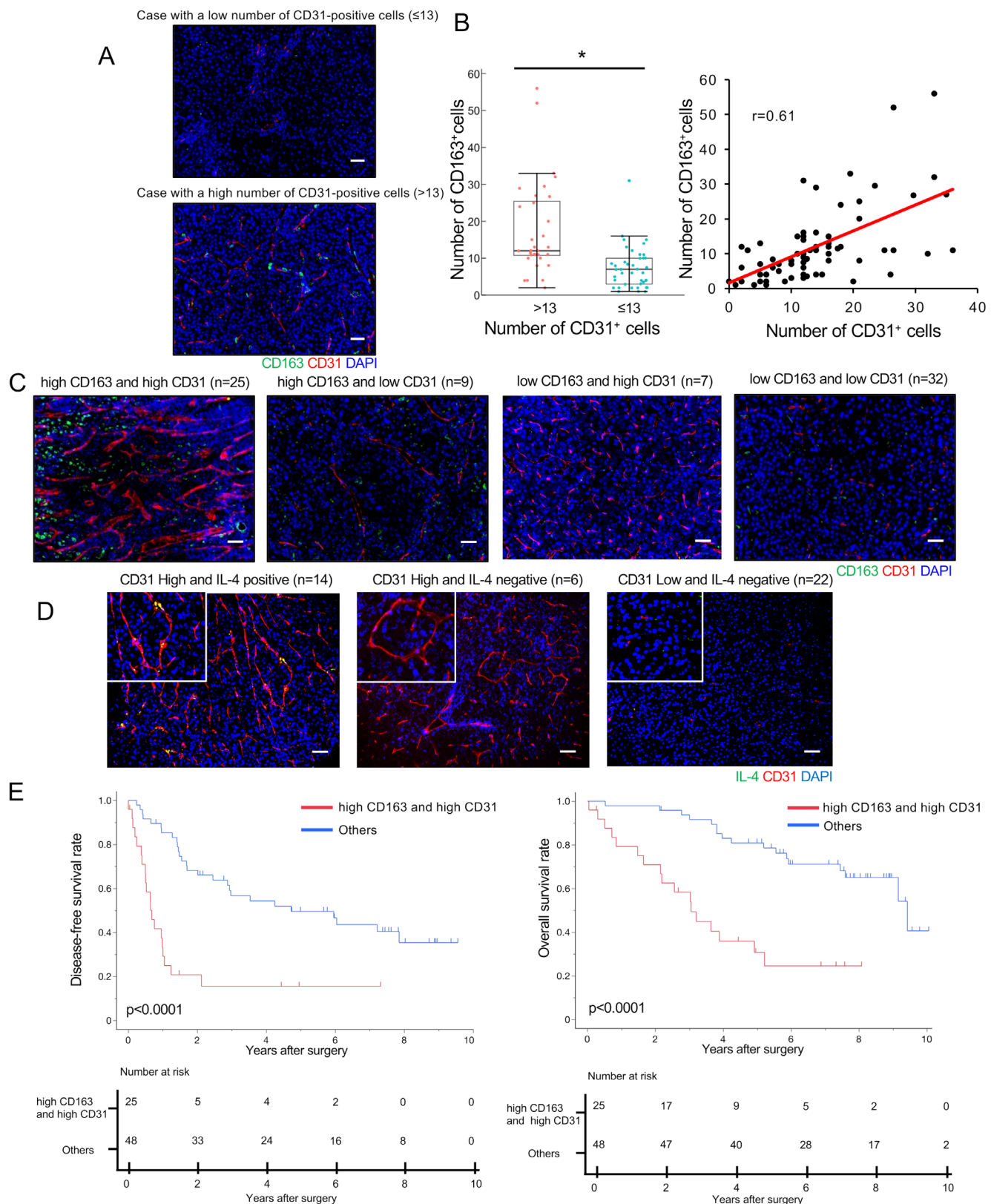


**FIGURE 5** | Analysis of the number of tumor blood vessels and M2 macrophages in HCC and the impact on patient prognosis. (A) Representative double immunofluorescent staining of cases with a low and high number of CD31<sup>+</sup> cells (scale bar, 100  $\mu$ m). (B) CD163<sup>+</sup> cells in cases with a low and high number of CD31<sup>+</sup> cells. A box-and-whisker diagram (left panel) and scatter plot analysis (right panel) are shown. (C) Representative double immunofluorescent staining of CD163 and CD31 in the four groups (scale bar, 50  $\mu$ m). (D) Representative double immunofluorescent staining of IL-4 and CD31 in the HCC patients (scale bar, 50  $\mu$ m). (E) Disease-free survival curves (left panel) and overall survival curves in the high CD163 and high CD31 group and others (right panel). \* $p < 0.05$ .

**TABLE 1** | Patient characteristics.

Variables	High CD163 and high CD31 group ( <i>n</i> = 25)	Others ( <i>n</i> = 48)	<i>p</i>
Age	69 (47–84)	53 (53–84)	0.730
Sex (male/female)	20/5	36/12	0.629
HBs-Ag (+/-)	3/22	6/42	0.951
Anti-HCV Ab (+/-)	15/10	24/24	0.415
Child-Pugh classification (A/B)	22/3	45/3	0.407
Platelet count ( $\times 10^4/\mu\text{L}$ )	13.3 (8.8–31.1)	14.6 (5.1–45.1)	0.731
Total bilirubin (mg/dL)	0.7 (0.4–1.1)	0.6 (0.3–1.3)	0.263
Prothrombin time (%)	80 (41–108)	86 (24–112)	0.221
AFP (ng/mL)	51 (3.0–26,101)	7 (2–36,143)	0.001
DCP (mAU/mL)	367 (13–361,200)	83 (1.3–88,400)	0.012
Tumor size (cm)	3.7 (1.4–32)	2.85 (0.8–15)	0.042
Number of tumor (multiple/single)	8/17	10/38	0.300
Histological type (poor/well, mod)	14/11	14/29	0.059
Microscopic vascular invasion (+) (%)	9 (36.0)	7 (14.5)	0.040
Microscopic im (+) (%)	8 (32.0)	8 (16.6)	0.140
Liver cirrhosis (+) (%)	10 (40.0)	22 (45.8)	0.633

Note: Data are presented as median (range) or *n* (%).

Abbreviations: AFP, alpha-fetoprotein; CEA, carcinoembryonic antigen; DCP, des-gamma-carboxy prothrombin; HCV, hepatitis C virus; im, intrahepatic metastasis.

**TABLE 2** | Univariate and multivariate analyses of overall survival.

Variables	Univariate			Multivariate		
	HR	95% CI	<i>p</i>	HR	95% CI	<i>p</i>
Age ( $\geq 70/< 70$ years)	1.099	0.557–2.170	0.786			
Sex (male/female)	2.209	0.844–5.787	0.107			
HBs-Ag (+/-)	0.329	0.078–1.384	0.129			
Anti-HCV Ab (+/-)	0.973	0.495–1.911	0.937			
Child-Pugh classification (B/A)	3.084	1.768–8.083	0.022	3.468	1.278–9.408	0.015
Platelet count ( $< 14/\geq 14 \times 10^4/\mu\text{L}$ )	1.702	0.851–3.404	0.133			
Total bilirubin ( $\geq 0.7/< 0.7$ mg/dL)	1.703	0.866–3.351	0.123			
Prothrombin time ( $\leq 70/> 70\%$ )	1.767	0.618–5.047	0.288			
AFP ( $\geq 200/< 200$ ng/mL)	1.185	0.505–2.783	0.697			
DCP ( $\geq 400/< 400$ mAU/mL)	1.572	0.785–3.151	0.202			
Tumor size ( $\geq 3/< 3$ cm)	1.409	0.709–2.803	0.328			
Number of tumor (multiple/single)	1.618	0.788–3.253	0.190			
Histological type (poor/well, mod)	1.430	0.718–2.849	0.309			
Microscopic vascular invasion (+/-)	2.791	0.967–8.052	0.058			
Microscopic im (+/-)	1.633	0.762–3.503	0.208			
Liver cirrhosis (+/-)	1.199	0.610–2.358	0.599			
CD163 and CD31 (high and high/others)	4.607	2.247–9.443	$< 0.001$	4.880	2.351–10.127	$< 0.001$

Abbreviations: AFP, alpha-fetoprotein; CEA, carcinoembryonic antigen; CI, confidence interval; DCP, des-gamma-carboxy prothrombin; HCV, hepatitis C virus; HR, hazard ratio; im, intrahepatic metastasis.

**TABLE 3** | Univariate and multivariate analyses of disease-free survival.

Variables	Univariate			Multivariate		
	HR	95% CI	p	HR	95% CI	p
Age ( $\geq 70$ / $< 70$ years)	0.736	0.410–1.321	0.304			
Sex (male/female)	1.143	0.567–2.303	0.709			
HBs-Ag (+/-)	0.799	0.315–2.026	0.637			
Anti-HCV Ab (+/-)	1.169	0.654–2.088	0.598			
Child-Pugh classification (B/A)	0.874	0.271–2.821	0.598			
Platelet count ( $< 14$ / $\geq 14 \times 10^4/\mu\text{L}$ )	1.550	0.868–2.765	0.138			
Total bilirubin ( $\geq 0.7$ / $< 0.7$ mg/dL)	1.185	0.668–2.105	0.562			
Prothrombin time ( $\leq 70$ / $> 70$ %)	1.739	0.685–4.410	0.244			
AFP ( $\geq 200$ / $< 200$ ng/mL)	1.875	0.949–3.704	0.070			
DCP ( $\geq 400$ / $< 400$ mAU/mL)	2.473	1.376–4.444	0.003	1.446	0.648–3.227	0.368
Tumor size ( $\geq 3$ / $< 3$ cm)	1.941	1.053–3.577	0.034	1.309	0.605–2.832	0.494
Number of tumor (multiple/single)	3.350	1.821–6.163	$< 0.001$	1.672	0.545–5.128	0.368
Histological type (poor/well, mod)	1.476	0.823–2.648	0.192			
Microscopic vascular invasion (+/-)	5.395	2.143–13.581	$< 0.001$	2.232	0.773–6.448	0.138
Microscopic im (+/-)	3.799	2.039–7.077	$< 0.001$	2.056	0.628–6.727	0.234
Liver cirrhosis (+/-)	1.607	0.905–2.857	0.106			
CD163 and CD31 (high and high/others)	3.765	2.050–6.915	$< 0.001$	3.358	1.734–6.500	$< 0.001$

Abbreviations: AFP, alpha-fetoprotein; CEA, carcinoembryonic antigen; CI, confidence interval; DCP, des-gamma-carboxy prothrombin; HCV, hepatitis C virus; HR, hazard ratio; im, intrahepatic metastasis.

IL-13, and TGF- $\beta$ 1 promote the polarization of TAMs towards the M2 type, which contributes to tumor progression through enhanced proliferation, invasion, and immune evasion by tumor cells [32, 33]. IL-4 and IL-4 receptor have also been associated with immunosuppressive effects within the TME and linked to poor prognosis in several cancers, including HCC [34]. IL-4/13 and IL-10 activate the M2 phenotype through signal transducer and activator of transcription 6 (STAT6) and STAT3, respectively [35]. In contrast, IFN- $\gamma$  orients macrophage polarization towards the M1 phenotype through activation of the STAT1 pathway. The balance between activation of STAT3/STAT6 versus STAT1 finely regulates macrophage expression and polarization [36]. In our study, we demonstrated that TEC-derived IL-4 plays a direct and major role in inducing M2 polarization of macrophages in HCC. Our findings show that TECs play an important role in secreting cytokines and forming the immunosuppressive TME in HCC. Our previous studies have shown that tumor vascular endothelial cells can promote CD8 $^{+}$  T-cell exhaustion via GPNMB expression [18]. Thus, TECs can suppress tumor immunity through various interactions with different types of immune cells.

In our analysis of resected HCC specimens, we found a positive correlation between CD31 $^{+}$  TECs and CD163 $^{+}$  M2 macrophages. Dividing patients into four groups based on the abundance of TECs and M2 macrophages, we found that HCC patients with a high number of both cells had an unfavorable prognosis.

These results support TECs inducing M2 polarization via IL-4. However, a small cohort had high CD31 $^{+}$  TECs but low CD163 $^{+}$  M2 macrophages. These results indicate a mechanism inhibiting M2 macrophage polarization. Possibilities include inadequate secretion of IL-4 from TECs, a dysfunction downstream of IL-4 signaling, and an imbalance between activation of STAT3/STAT6 versus STAT1. We also found a cohort of HCC patients with low levels of CD31 $^{+}$  TECs and high levels of CD163 $^{+}$  M2 macrophages. In general, macrophage polarization to M1 or M2 is regulated by many different microenvironmental stimuli. The M1 phenotype is stimulated by microbial products, such as lipopolysaccharide, or pro-inflammatory cytokines, such as IFN- $\gamma$ , tumor necrosis factor, and Toll-like receptor ligands. M2 macrophages are induced by Th2 cytokines IL-4, IL-10, and IL-13 [37, 38]. Macrophage polarization is defined by the balance of these stimuli, and M2 macrophage polarization was stimulated by other cytokines from cancer cells or the TME in the cohort with low levels of TECs and high levels of M2 macrophages [39, 40]. Our results indicate that there are various and complex intracellular interactions within TAMs, TECs, and other types of cells in the TME, and this study demonstrated one aspect of the molecular mechanism of M2 macrophage polarization between TAMs and TECs. Further studies are needed to clarify TME interactions in HCC.

In conclusion, our study demonstrates that TECs induce M2 macrophage polarization through IL-4 secretion, leading to



immune suppression and cancer progression. A high number of both TECs and M2 macrophages correlates with poor prognosis in HCC. IL-4 secretion by TECs is a potential therapeutic target for HCC.

## Author Contributions

**Daijiro Matoba:** data curation, formal analysis, investigation, methodology, visualization, writing – original draft, writing – review and editing. **Takehiro Noda:** conceptualization, formal analysis, methodology, project administration, writing – review and editing. **Shogo Kobayashi:** resources, writing – review and editing. **Yoshihiro Sakano:** data curation, investigation, writing – review and editing. **Kenichi Matsumoto:** data curation, writing – review and editing. **Chihiro Yamanaka:** data curation, writing – review and editing. **Kazuki Sasaki:** formal analysis, writing – review and editing. **Shinichiro Hasegawa:** data curation, writing – review and editing. **Yoshifumi Iwagami:** formal analysis, writing – review and editing. **Daisaku Yamada:** methodology, writing – review and editing. **Yoshito Tomimaru:** resources, writing – review and editing. **Hirofumi Akita:** data curation, writing – review and editing. **Hidegori Takahashi:** resources, writing – review and editing. **Tadafumi Asaoka:** data curation, writing – review and editing. **Junzo Shimizu:** data curation, writing – review and editing. **Hisashi Wada:** funding acquisition, supervision, writing – review and editing. **Yuichiro Doki:** funding acquisition, supervision, writing – review and editing. **Hidetoshi Eguchi:** funding acquisition, supervision, writing – review and editing.

## Ethics Statement

Approval of the Research Protocol by an Institutional Review Board: The use of resected samples and clinicopathological data for this study was approved by the Human Ethics Review Committee of The University of Osaka (24386).

Animal Studies: This study was approved by the Animal Experiments Committee, The University of Osaka (approval number 05-006-003).

## Consent

All patients gave written informed consent for research use of their surgical specimens and clinicopathological data; patient anonymity was preserved.

## Conflicts of Interest

The Department of Clinical Research in Tumor Immunology is a collaborating laboratory of the University of Osaka and Shionogi Co. Ltd. The authors declare no conflicts of interest.

## References

1. H. Sung, J. Ferlay, R. L. Siegel, et al., “Global Cancer Statistics 2020: GLOBOCAN Estimates of Incidence and Mortality Worldwide for 36 Cancers in 185 Countries,” *CA: A Cancer Journal for Clinicians* 71 (2021): 209–249.
2. T. Noda, Y. Sasaki, T. Yamada, et al., “Usefulness of the CLIP Scoring System for Prediction of Postoperative Prognosis of Patients With Large Hepatocellular Carcinoma,” *Journal of Hepato-Biliary-Pancreatic Surgery* 16 (2009): 538–545.
3. T. Noda, H. Nagano, Y. Tomimaru, et al., “Prognosis of Hepatocellular Carcinoma With Biliary Tumor Thrombi After Liver Surgery,” *Surgery* 149 (2011): 371–377.
4. R. S. Finn, S. Qin, M. Ikeda, et al., “Atezolizumab Plus Bevacizumab in Unresectable Hepatocellular Carcinoma,” *New England Journal of Medicine* 382 (2020): 1894–1905.

5. Y. H. Wu, J. G. Cao, H. L. Xiang, et al., “Recombinant Vascular Basement-Membrane-Derived Multifunctional Peptide Inhibits Angiogenesis and Growth of Hepatocellular Carcinoma,” *World Journal of Gastroenterology* 15 (2009): 1744–1750.
6. C. Chen, Z. Wang, Y. Ding, and Y. Qin, “Tumor Microenvironment-Mediated Immune Evasion in Hepatocellular Carcinoma,” *Frontiers in Immunology* 14 (2023): 1133308.
7. M. Kudo, “New Treatment Paradigm With Systemic Therapy in Intermediate-Stage Hepatocellular Carcinoma,” *International Journal of Clinical Oncology* 27 (2022): 1110–1119.
8. A. Taketomi, “Clinical Trials of Antiangiogenic Therapy for Hepatocellular Carcinoma,” *International Journal of Clinical Oncology* 21 (2016): 213–218.
9. K. Cheng, N. Cai, J. Zhu, X. Yang, H. Liang, and W. Zhang, “Tumor-Associated Macrophages in Liver Cancer: From Mechanisms to Therapy,” *Cancer Commun (Lond)* 42 (2022): 1112–1140.
10. K. Wu, K. Lin, X. Li, et al., “Redefining Tumor-Associated Macrophage Subpopulations and Functions in the Tumor Microenvironment,” *Frontiers in Immunology* 11 (2020): 1731.
11. Z. Li, T. Wu, B. Zheng, and L. Chen, “Individualized Precision Treatment: Targeting TAM in HCC,” *Cancer Letters* 458 (2019): 86–91.
12. O. W. H. Yeung, C.-M. Lo, C.-C. Ling, et al., “Alternatively Activated (M2) Macrophages Promote Tumour Growth and Invasiveness in Hepatocellular Carcinoma,” *Journal of Hepatology* 62 (2015): 607–616.
13. K. Hida, T. Kawamoto, N. Ohga, K. Akiyama, Y. Hida, and M. Shin-doh, “Altered Angiogenesis in the Tumor Microenvironment,” *Pathology International* 61 (2011): 630–637.
14. K. Kato, T. Noda, S. Kobayashi, et al., “KLK10 Derived From Tumor Endothelial Cells Accelerates Colon Cancer Cell Proliferation and Hematogenous Liver Metastasis Formation,” *Cancer Science* 115 (2024): 1520–1535.
15. N. Maishi and K. Hida, “Tumor Endothelial Cells Accelerate Tumor Metastasis,” *Cancer Science* 108 (2017): 1921–1926.
16. R. K. Jain, “Normalization of Tumor Vasculature: An Emerging Concept in Antiangiogenic Therapy,” *Science* 307 (2005): 58–62.
17. K. Matsumoto, T. Noda, S. Kobayashi, et al., “Inhibition of Glycolytic Activator PFKFB3 Suppresses Tumor Growth and Induces Tumor Vessel Normalization in Hepatocellular Carcinoma,” *Cancer Letters* 500 (2021): 29–40.
18. Y. Sakano, T. Noda, S. Kobayashi, et al., “Tumor Endothelial Cell-Induced CD8(+) T-Cell Exhaustion via GPNMB in Hepatocellular Carcinoma,” *Cancer Science* 113 (2022): 1625–1638.
19. G. Shinke, D. Yamada, H. Eguchi, et al., “Role of Histone Deacetylase 1 in Distant Metastasis of Pancreatic Ductal Cancer,” *Cancer Science* 109 (2018): 2520–2531.
20. T. Noda, H. Nagano, I. Takemasa, et al., “Activation of Wnt/Beta-Catenin Signalling Pathway Induces Chemoresistance to Interferon-Alpha/5-Fluorouracil Combination Therapy for Hepatocellular Carcinoma,” *British Journal of Cancer* 100 (2009): 1647–1658.
21. M. Mikamori, D. Yamada, H. Eguchi, et al., “MicroRNA-155 Controls Exosome Synthesis and Promotes Gemcitabine Resistance in Pancreatic Ductal Adenocarcinoma,” *Scientific Reports* 7 (2017): 42339.
22. S. Wang, J. Wang, Z. Chen, et al., “Targeting M2-Like Tumor-Associated Macrophages Is a Potential Therapeutic Approach to Overcome Antitumor Drug Resistance,” *NPJ Precision Oncology* 8 (2024): 31.
23. R. Noy and J. W. Pollard, “Tumor-Associated Macrophages: From Mechanisms to Therapy,” *Immunity* 41 (2014): 49–61.
24. T. Noda, H. Yamamoto, I. Takemasa, et al., “PLOD2 Induced Under Hypoxia Is a Novel Prognostic Factor for Hepatocellular Carcinoma After Curative Resection,” *Liver International* 32 (2011): 110–118.



25. X. D. Zhu, J. B. Zhang, P. Y. Zhuang, et al., "High Expression of Macrophage Colony-Stimulating Factor in Peritumoral Liver Tissue Is Associated With Poor Survival After Curative Resection of Hepatocellular Carcinoma," *Journal of Clinical Oncology* 26 (2008): 2707–2716.
26. T. Ding, J. Xu, F. Wang, et al., "High Tumor-Infiltrating Macrophage Density Predicts Poor Prognosis in Patients With Primary Hepatocellular Carcinoma After Resection," *Human Pathology* 40 (2009): 381–389.
27. S. Wang, G. Liu, Y. Li, and Y. Pan, "Metabolic Reprogramming Induces Macrophage Polarization in the Tumor Microenvironment," *Frontiers in Immunology* 13 (2022): 840029.
28. Z. Ge and S. Ding, "The Crosstalk Between Tumor-Associated Macrophages (TAMs) and Tumor Cells and the Corresponding Targeted Therapy," *Frontiers in Oncology* 10 (2020): 590941.
29. Y. Waki, Y. Morine, Y. Saito, et al., "Lenvatinib-Resistant Hepatocellular Carcinoma Promotes Malignant Potential of Tumor-Associated Macrophages via Exosomal miR-301a-3p," *Annals of Gastroenterological Surgery* 8 (2024): 1084–1095.
30. Y. Huang, J. Yuan, E. Righi, et al., "Vascular Normalizing Doses of Antiangiogenic Treatment Reprogram the Immunosuppressive Tumor Microenvironment and Enhance Immunotherapy," *Proceedings of the National Academy of Sciences of the United States of America* 109 (2012): 17561–17566.
31. C. Rolny, M. Mazzone, S. Tugues, et al., "HRG Inhibits Tumor Growth and Metastasis by Inducing Macrophage Polarization and Vessel Normalization Through Downregulation of PlGF," *Cancer Cell* 19 (2011): 31–44.
32. A. Suzuki, P. Leland, B. H. Joshi, and R. K. Puri, "Targeting of IL-4 and IL-13 Receptors for Cancer Therapy," *Cytokine* 75 (2015): 79–88.
33. V. Gocheva, H. W. Wang, B. B. Gadea, et al., "IL-4 Induces Cathepsin Protease Activity in Tumor-Associated Macrophages to Promote Cancer Growth and Invasion," *Genes & Development* 24 (2010): 241–255.
34. C. Guo, Y. Ouyang, J. Cai, et al., "High Expression of IL-4R Enhances Proliferation and Invasion of Hepatocellular Carcinoma Cells," *International Journal of Biological Markers* 32 (2017): e384–e390.
35. K. Wu, I. Kryczek, L. Chen, W. Zou, and T. H. Welling, "Kupffer Cell Suppression of CD8+ T Cells in Human Hepatocellular Carcinoma Is Mediated by B7-H1/Programmed Death-1 Interactions," *Cancer Research* 69 (2009): 8067–8075.
36. A. Sica, P. Invernizzi, and A. Mantovani, "Macrophage Plasticity and Polarization in Liver Homeostasis and Pathology," *Hepatology* 59 (2014): 2034–2042.
37. D. Li, T. Zhang, Y. Guo, C. Bi, M. Liu, and G. Wang, "Biological Impact and Therapeutic Implication of Tumor-Associated Macrophages in Hepatocellular Carcinoma," *Cell Death & Disease* 15 (2024): 498.
38. H. Zheng, X. Peng, S. Yang, et al., "Targeting Tumor-Associated Macrophages in Hepatocellular Carcinoma: Biology, Strategy, and Immunotherapy," *Cell Death Discovery* 9 (2023): 65.
39. M. Yu, H. Yu, H. Wang, et al., "Tumor-Associated Macrophages Activated in the Tumor Environment of Hepatocellular Carcinoma: Characterization and Treatment (Review)," *International Journal of Oncology* 65 (2024): 100.
40. K. Shirabe, Y. Mano, J. Muto, et al., "Role of Tumor-Associated Macrophages in the Progression of Hepatocellular Carcinoma," *Surgery Today* 42 (2012): 1–7.

## Supporting Information

Additional supporting information can be found online in the Supporting Information section. **Figure S1:** Gating strategy for identification of macrophages by flow cytometry. (A) In vitro cultured macrophages were gated by exclusion of dead cells using a viability dye, followed by sequential gating on CD11b<sup>+</sup>F4/80<sup>+</sup> cells. (B) Tumor-infiltrating

macrophages from in vivo samples were gated by excluding dead cells, then selecting CD45<sup>+</sup> leukocytes, followed by gating on CD11b<sup>+</sup>F4/80<sup>+</sup> macrophages. **Figure S2:** The analysis of intratumoral macrophages. (A) Double immunofluorescent staining of CD31 and F4/80 in BNL-T, BNL-T+NEC, and BNL-T+TEC tumors. Nuclei were counterstained with DAPI (scale bars, 100 μm). Quantification of F4/80-positive cells in the tumor (right) (B) Double immunofluorescent staining of CD31 and F4/80 in BNL-T+TEC with scramble siRNA and BNL-T+TEC with IL-4 siRNA tumors. Nuclei were counterstained with DAPI (scale bars, 100 μm). Quantification of F4/80-positive cells in the tumor (right) Mean ± SEM. n.s; *p* > 0.05. **Figure S3:** Analysis of the number of tumor blood vessels and M2 macrophages in HCC and the impact on patient prognosis. Disease-free survival curves (left panel) and overall survival curves (right panel) for the four groups (high CD163 and high CD31, high CD163 and low CD31, low CD163 and high CD31, and low CD163 and low CD31). **Figure S4:** Analysis of the number of tumor blood vessels and CD206-positive M2 macrophages in HCC and the impact on patient prognosis. (A) Representative double immunofluorescent staining of CD206 and CD31 in the four groups (scale bar, 50 μm). (B) Disease-free survival curves (left panel) and overall survival curves in the high CD206 and high CD31 group and others (right panel).